6ICEGE
6th International Conference on Earthquake Geotechnical Engineering
1-4 November 2015
Christchurch, New Zealand

Centrifuge Modeling of Seismic Behavior of Caisson-Supported Subsea Manifold on Soft Clay

B.L. Zheng[1], B.L. Kutter[2], G.S. Hirt[3], Y.G. Zhou[4], D.W. Wilson[5], E.C. Clukey[6]

ABSTRACT

Subsea manifolds serve as central collection points for transfer of gas from nearby wellheads via seafloor jumpers. Use of caisson foundations over conventional piles is common for manifolds founded on soft seabeds. The seismic behavior of caisson-supported subsea manifolds on soft clay is not well-understood. Consequently, a centrifuge test was conducted at the Center for Geotechnical Modeling at UC Davis to study the seismic response of a caisson-supported manifold structure and a deeply-installed wellhead founded on soft clay when subjected to extreme and abnormal level earthquakes. The paper discusses the layout of the soil model and key design aspects of the manifold structure. Partial results are presented to illustrate site response in soft clay deposits, rocking behavior of caisson foundation, relative displacement and deformation envelopes of the manifold, wellhead and free-field extracted from generated animations of the transient response, and moment- and settlement-rotation of the manifold.

Introduction

Deep wells founded on soft, subsea soil beds extract gas from reservoirs. Commonly, the product from a number of wells is collected at a central manifold on the sea bed via jumper connections resting on the seabed (see Figure 1(a) and (b)). Subsea soils sometimes consist of deep deposits of normally consolidated or lightly over-consolidated, high plasticity clay. To support the manifold on such soft clay deposits, caisson foundations are often used. However, no data is available from field case histories to show how these foundation-jumper-well systems perform during seismic shaking.

A centrifuge test program was devised to provide the needed data. In addition to facilitating improved understanding of the problem, the data is to be used to validate the numerical procedures used to analyze the seismic performance of subsea manifolds on caisson foundations. Centrifuge modeling has been used by many researchers to study the installation process (Andersen et al., 2004) and tension capacity (Chen and Randolph, 2005, and Jeanjean et al., 2006) of individual caissons. However, no known work has been done in the centrifuge to model the seismic and lateral behavior of caisson-supported structures.

A scale model of a wellhead-jumper-manifold system in soft clay was subjected to ALE (abnormal) and ELE (extreme level earthquakes) on the centrifuge to produce data to test the methods of analysis used in practice. Details of the centrifuge test are summarized in the data

[1] Graduate Student, Civil & Environmental Engineering, UC Davis, USA, baozheng@ucdavis.edu
[2] Professor, Civil & Environmental Engineering, UC Davis, USA, blkutter@ucdavis.edu
[3] Graduate Student, Civil & Environmental Engineering, UC Davis, USA, gshirt@ucdavis.edu
[4] Associate Professor, Civil Engineering, Zhejiang University, P. R. China, qzking@zju.edu.cn
[5] Research Faculty, Civil & Environmental Engineering, UC Davis, USA, dxwilson@ucdavis.edu
[6] Geotechnical Advisor, BP America, Houston, USA, edward.clukey@bp.com

report by Zheng et al. (2014). In this paper, important design aspects and results are discussed and presented.

Centrifuge Model Layout

The centrifuge model was assembled in the "hinged plate" container (HPC) at the UC Davis Center for Geotechnical Modeling. A drawing of the HPC is shown in Figure 1(c). The HPC has measured internal dimensions of 1756 mm in length by 649 mm in width by 516 mm deep. A rubber liner (3 mm thick) was placed within the container to prevent leakage of pore fluid. Inside the liner on the north and south ends of the container, a series of vertical studding rods were installed to provide the required complementary shear stresses at these boundaries.

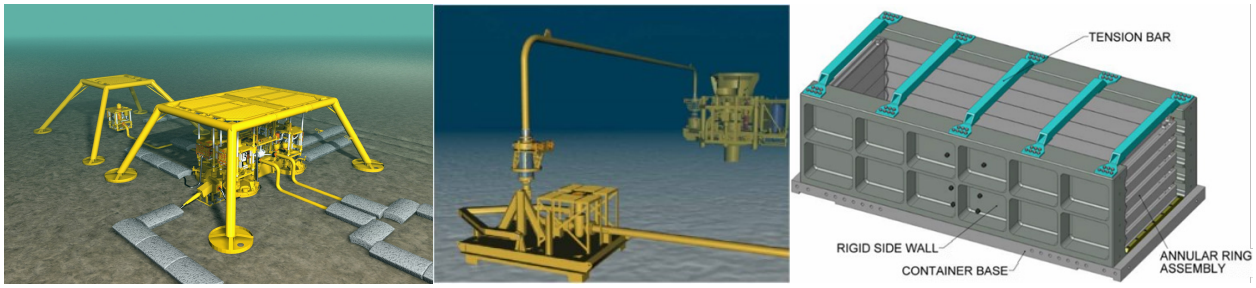

(a) (b) (c)

Figure 1. Jumper connections between the manifold and the wellhead. Jumper behavior is governed by the displacements between (a) the manifold and the wellhead relative to free-field surface ("Photo Gallery", 2009), and (b) directly between the manifold and the wellhead (Lacour, 2015). (c) Drawing of the hinged plate model container on the centrifuge.

The model was constructed in alternating thick layers of clay and thin layers of sand, as shown in Figure 2. Dimensions are presented in prototype scale, using a scale factor of 58 (or 58 g) between model and the prototype. Kaolin clay was used for the base layer, and mixed clay of 20% natural clay and 80% kaolin by mass was used for the upper clay layers. Selection of this composition is discussed later. Clay layers were consolidated in 8 sublayers in a hydraulic press to pre-consolidate the soil before loading on the centrifuge. Target consolidation stresses were set to equal the expected vertical stresses at the base of the respective sublayers at 58 g. The ultimate OCR profile at 58 g was lightly over-consolidated ($1 \leq OCR \leq 1.4$).

Base and intermediate sand drains were placed in the model to increase the rate of consolidation. A thin layer of Nevada sand was placed as a base drainage boundary along the length of the container, which extended into vertical side drains on the north and south ends of the container. Three additional intermediate layers of Nevada sand were pluviated on top of the kaolin base layer and after each subsequent layer of clay mixture. Relative densities were approximately 85% for the base layer and 80% for the side and intermediate drains.

Properties of soils used in the experiment are reported in Table 1. The high plasticity natural clay had a very small coefficient of consolidation that would preclude drainage during the centrifuge test. Kaolin was mixed with the natural clay to produce a suitable model clay that would consolidate in a practical time period. A clay mixture composition of 20% natural clay and 80%

kaolin was selected based on a design constraint that 95% consolidation should occur in 7 hours. The density of kaolin is higher than the natural clay, hence the vertical stress and strength increase with depth were also greater than that of the natural soil.

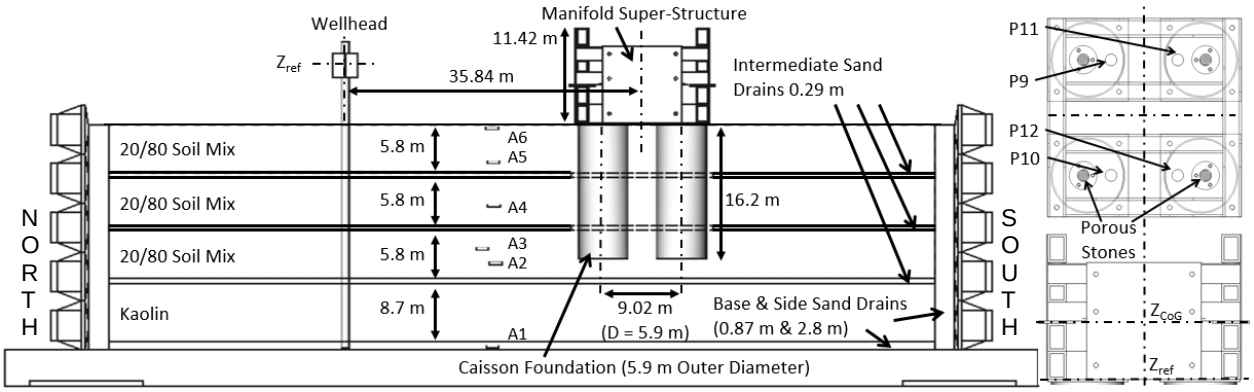

Figure 2. Model layout showing locations of the manifold, wellhead, clay layers, and sand drains. Drains bounded by dashed line indicate discontinuity in the east-west direction.

The manifold and caisson geometry, drawn to scale in Figure 2, is based on a preliminary design of an actual subsea installation. However, to compensate for the increase in soil strength described above, the mass of the manifold structure was increased by 35% in the model test.

Table 1. Selected parameters for the sand and clay used in the test.

	Units	Kaolin	Nevada Sand	20/80 Mixture
Grain Size (D_{50}, D_{10})	μm		170 [b], 100 [b]	
Specific Gravity, G_s			2.67 [c]	2.6 [d]
Atterberg Indices (PL, LL)	%	28.3 [a], 46.8 [a]		32.0 [d], 60.1 [d]
C_v (λ, κ)	mm^2/s	0.7 [a], 2.3 [a]		0.07 [d], 0.26 [d]
Void Ratios (e_{min}, e_{max})			0.533 [c], 0.888 [c]	

[a] Stringer *et al.* (2012), [b] Kulasingam (2003), [c] Brandenberg *et al.* (2001), [d] Zheng *et al.* (2014).

Drainage Control for Caissons

The anticipated situation for suction caissons in the prototype is that the pore pressure inside the top of the caissons dissipate after installation, but the top of the caissons is sealed so that they would behave as if being undrained during seismic loading. To emulate this situation, a low-permeability ceramic porous stone was installed to allow pore pressures generated during spin-up of the centrifuge to be dissipated prior to seismic loading, with the constraint that the drainage rate would be slow enough to preclude significant drainage during seismic shaking. Pore pressure transducers (PPT) were installed next to the porous stones to monitor pore pressures at the top of the caissons during the test. Plan view of the setup is provided in Figure 2.

Axial Capacity of Caisson Foundation

The manifold structure was driven into the soil model at 1 g using dead weight. There was concern about the undrained axial stability of the structure during spin-up to 58 g. As the

centrifugal force increases with spin-up, the weight of the structure increases proportionally. However, because the strength of the soil increases slowly with consolidation, the soil might be unable to support the weight of the structure at high g levels, before consolidation is complete. The factor of safety against compression failure was evaluated for cases of undrained soil strength before and after consolidation at 58 g, with and without plugging of the caissons, using Equations 1 and 2. Results are summarized in Table 2. When the caissons are plugged, the weight of the contained soil contributes to the load, and end bearing is assumed over the total area of the caisson. For the unplugged case, there is friction on the inside and outside surfaces of the caisson, but the end bearing only applies to the annulus. Zheng et al. (2014) provides all the information to determine the parameters for Equations 1 and 2.

$$FS_{Plugging} = \frac{N_c S_{u,Ng_{base}} A_o + \sum_j^n \alpha_j \overline{S_{u,Ng_j}} D_o L_j + a^* \gamma_{soil} L_{caisson} A_o}{(a^* g)(m_{SS} + m_{Foundation}) / n_{caissons} + a^* \gamma_{soil} L_{caisson} A_i} \quad (1)$$

$$FS_{Non-Plugging} = \frac{N_c S_{u,Ng_{base}} (A_o - A_i) + 2\left(\sum_j^n \alpha_j \overline{S_{u,Ng_j}} D_o L_j\right) + a^* \gamma_{soil} L_{caisson} (A_o - A_i)}{(a^* g)(m_{SS} + m_{Foundation}) / n_{caissons}} \quad (2)$$

In the above equations, N_c is the end bearing capacity factor and the value of 9 was adopted from a caisson design example from Houlsby and Byrne (2004), $S_{u, Ng}$ is the undrained strength of soil, A_o, A_i, D_o, and $L_{caisson}$ are the outer and inner cross-sectional areas, outer diameter, and length of the caissons, α is the adhesion factor from API (2000), γ_{soil} is the density of the soil at 1 g, a^* is the prototype-to-model scale factor for acceleration, m_{SS} and $m_{Foundation}$ are the model scale masses of the super-structure and foundation, and $n_{caissons}$ is the number of caissons. A factor of 2 is applied to the shaft capacity in Equation 2 to account for the interior shaft friction, assuming it is the same as the exterior shaft friction. Computed factors of safety were greater than 1; compression failure was not expected to occur.

Table 2. Factor of safety against compression failure.

	Prototype	Model, $a^* = a_{model}/a_{prototype} = 58$	
Undrained strength, $S_{u,Ng}$	Prototype	Consolidated-Undrained	Unconsolidated-Undrained
		Factors of Safety	
Plugging (Equation 1)	1.8	2.2	1.4
Non-plugging (Equation 2)	2.4	3.5	1.8

Results

Three motions were applied to the centrifuge model: one extreme level earthquake, ELE, and two abnormal level earthquakes, ALE-#1 and ALE-#2. Results presented in paper are primarily for Motion ALE-#1 and have been converted to prototype scale, using the scale factor of 58 and following the scaling laws summarized in Garnier et al. (2007).

Site response in soft clay was studied using measurements from the base and free-field accelerometers, A1-A6, labeled in Figure 2. Measurements for Motion ALE-#1 are presented in

Figure 3(a). A peak acceleration of 0.615 g was recorded at the base. The response attenuated with elevation to a peak accelerations of 0.209 g at the surface. Acceleration and displacement response spectra for 5% critical damping at the base and surface are shown in Figure 3(b) for all three applied motions. For Motion ELE, minor softening and attenuation is observed. For Motions ALE-#1 and ALE-#2, significant softening and attenuation can be seen by the increase in predominant period, reduction of spectral acceleration, and increase in spectral displacement.

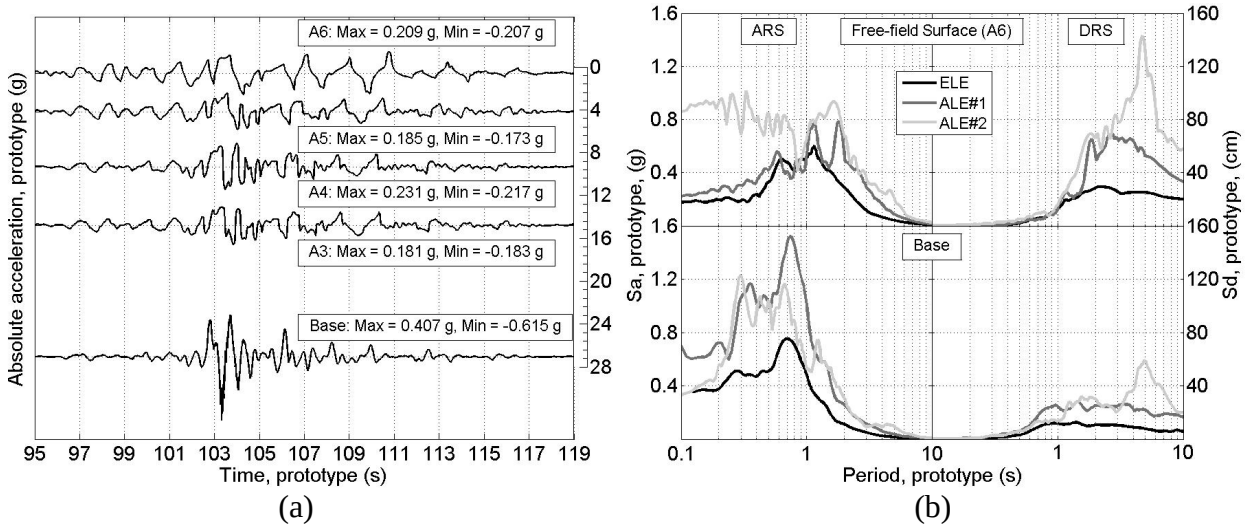

(a) (b)

Figure 3. (a) Free-field response during Motion ALE-#1. Vertical separation of traces is proportional to the vertical distances between the sensors. Depth of sensor from ground surface is given on right side of time series plot. (b) Acceleration and displacement response spectra of the base and free-field surface for 5% critical damping.

Pore pressure time histories for PPT P9 to P12 (shown in Figure 2) are presented in Figure 4. Excess pore pressures of 10 to 15 kPa were measured inside the caissons just below the top plates. If all the structure mass was transferred to the excess pore pressure, the increase would have been 112 kPa. Cyclic excess pore pressures generated by the caissons on the north and south end of manifold structure are out-of-phase, which indicates that as one pair of caissons was loaded in cyclic compression, the other pair was in cyclic tension. The lack of pore pressure dissipation up to 120 seconds indicates that the pore pressures did not drain significantly during shaking, as desired. The right side of the figure, with different time scale to show the post-shake dissipation, shows that excess pore pressures in some of the caissons drained faster than others.

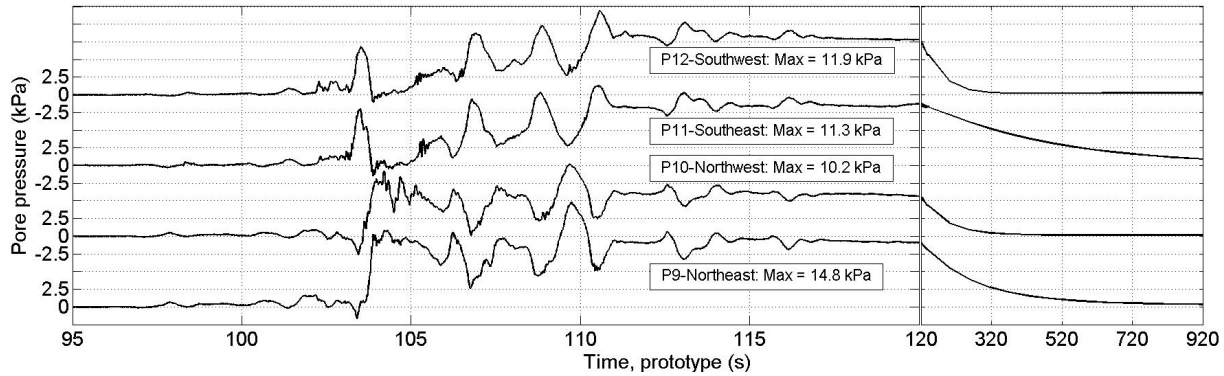

Figure 4. Pore pressure measurements inside the top of caissons during Motion ALE-#1.

Dynamic displacements are computed by integration of accelerometer recorded time histories. Base line correction used a 4th order non-causal high-pass Butterworth filter with zero phase-shift, and a corner frequency of 0.0862 Hz in prototype scale. The top plot in Figure 5 shows the displacements at the center-of-gravity of the manifold super-structure and the reference on the wellhead (See Figure 2) relative to free-field surface (sensor A6). Peak relative displacements are 13 cm and 33 cm, respectively. This comparison illustrates the behavior of the jumper connection shown in Figure 1(a), where the jumper behavior is governed by the relative displacement between the manifold and the wellhead to the free-field surface. Under Motion ALE-#1, the wellhead is the critical structure. The deformation of the jumpers connecting the manifold and the wellhead can be observed as the difference between the two curves shown at the top of Figure 5. The peak relative displacement is about 35 cm at 104.5 seconds, which is similar in magnitude to the relative displacement between the wellhead and free-field surface.

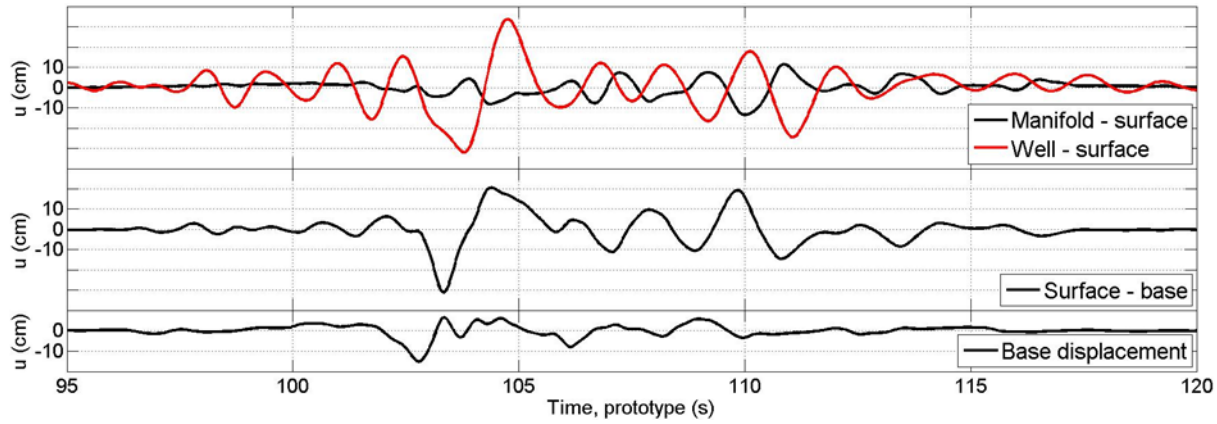

Figure 5. Horizontal displacements at the center of gravity of the manifold and the reference on the wellhead relative to free-field surface, and the free-field surface displacement relative to the base, for Motion ALE-#1. The integrated base displacement is shown at the bottom.

Deformations for the manifold and the wellhead were computed for Motion ALE-#1 using integrated displacements from accelerometers and assuming rigid-body rotation for the manifold and the caisson foundation. The maximum relative displacement in both directions for the manifold and wellhead and the envelope of maximum relative displacement of the soil column (all magnified by a factor of 5) are indicated by dark black lines in Figure 6(a). Animations

showing the full transient response during the motions are created, but cannot presented in this paper. The thin rectangular attachments to the manifold and the wellhead are representations of the jumper connections, which were not physically modeled in the centrifuge test. From the deformation envelopes of the manifold structure, the center of rotation of the foundation was below the tip of the caissons. The lack of symmetry of the rotation and displacement are expected based on the large pulse in the base motion (see Figure 5). Figure 6(b) shows a snapshot of the deformations between the caisson foundation and free-field soil column at the times of maximum and minimum foundation deformation. The displacement of free-field intersected the foundation displacement at about 20% to 50% of the length of the caisson below the top of the foundation, indicating the foundation was moving with the free-field at this depth. The shear strains in the free-field are shown as the relative displacements between sensors over their vertical separations. The rotation of the foundation was slightly less than the shear strain in the free-field along the length of the foundation. Figure 6(c) shows the normalized moment-rotation and normalized settlement-rotation of the manifold super-structure during Motion ALE-#1. Settlement of the manifold, w, is normalized by the outer edge-to-edge width of the caissons, assuming block failure for the caisson foundation. The applied moment is computed from mass times acceleration times height of the CoG of the super-structure normalized by the moment capacity, computed as the weight of the super-structure times the center-to-edge width of the block. Maximum rotation was 0.0085 radians counter-clockwise about the east-west axis and normalized residual settlement was 0.16%. The applied moment reached about 30% of the calculated moment capacity. Hysteretic behavior of the manifold structure can be observed from moment-rotation.

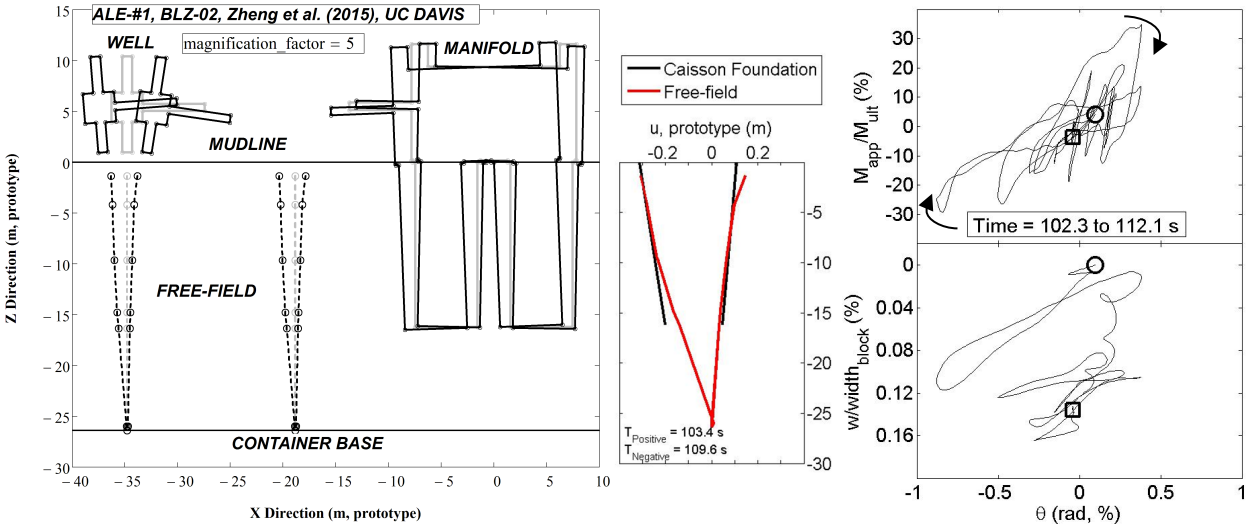

Figure 6. (a) Seismic deformation envelopes of the manifold structure, wellhead, and free-field during Motion ALE-#1, in black and magnified 5 times. (b) Snapshot of deformations of the caisson foundations and free-field at times of maximum and minimum foundation deformations. (c) Normalized moment-rotation and settlement-rotation of the super-structure. The starting point and ending points are marked by a circle and a square respectively.

Conclusion

A centrifuge test was conducted to produce some data regarding behavior of well-jumper-manifold systems. The data is to be used to validate methods of analysis used in practice.

The centrifuge model was constructed using substitute clay with lower PI and higher density than the prototype to reduce the time for consolidation during the centrifuge test. Porous stones were installed at the top of the caissons to allow caissons to be drained during installation and centrifuge spin-up, but undrained during the time scale of seismic loading. Factors of safety were computed to check the stability of the manifold structure against bearing failure. Compression failure was not expected. Factors are reasonably close to the typical values for prototype manifold systems.

Free-field dynamic response and pore pressure measurements inside the caissons are presented. Motions ALE-#1 and ALE-#2 caused attenuation of acceleration and soil softening with elevation. However, displacement was amplified with elevation. Measurements of excess pore pressures at the top of the caissons shows out-of-phase response of the PPTs between the north and south pairs of caissons, which is indicative of rocking response. Dynamic displacements at the center-of-gravity of the manifold structure and the reference point on the wellhead relative to the surface of the free-field are significant (13 cm and 33 cm respectively). Amplified deformed envelopes of manifold structure, the wellhead, and free-field are shown. The rotation of the caissons was slightly less than the average shear strain in the soil along the length of the caisson, and the lateral displacement of the caisson tended to follow the soil. Peak manifold rotation was 0.0085 radians, at which point about 30% of the estimated moment capacity was mobilized. Residual settlement of the foundation was about 0.16% of the width of the caisson foundation.

Acknowledgments

The support from our industry sponsor is gratefully acknowledged. We also appreciate the advice and assistance from the following staff and students of the UC Davis CGM: Chad Justice, Anatoliy Ganchenko, Tom Khonke, Lars Pedersen, Jacquelyn Allmond, Manny Hakhamaneshi, Andreas Gavras, Mohammad Khosravi, Yong Zhi Wang, and Mark Stringer. Dr. Y. G. Zhou was supported by the Foundation for the Author of National Excellent Doctoral Dissertation of P. R. China (No. 201160), the National Program for Special Support of Top-Notch Young Professionals (2012).

References

Andersen, K.H., Jeanjean, P., Luger, D., Jostad, H.P. (2004). "Centrifuge Tests on Installation of Suction Anchors in Soft Clay." *Ocean Engineering*, **32**, 845-863.

API (2000). *Recommended Practice for Planning, Designing, and Constructing Fixed Offshore Platforms – Working Stress Design, API RP-2A.* American Petroleum Institute.

Brandenberg, S., Singh, P., Boulanger, R.W., Kutter, B.L. (2001). "*Behaviour of Piles in Laterally Spreading Ground during Earthquakes - Centrifuge Data Report for SJB01*." *Technical Report*, University of California, Davis.

Chen, W., Randolph, M.F. (2005). "Centrifuge Tests on Axial Capacity of Suction Caissons in Clay." *Proceedings, International Symposium on Frontiers in Offshore Geotechnics*, 243-249.

Garnier, J., Gaudin, C., Springman, S.M., Culligan, P.J., Goodings, D., Konig, D., Kutter, B.L., Phillips, R., Randolph, M. F., Thorel, L. (2007). "Catalogue of Scaling Laws and Similitude Questions in Geotechnical Centrifuge Modelling." *International Journal of Physical Modelling in Geotechnics*, **3**, 1-23.

Houlsby, G.T., Byrne, B.W. (2005). "Design Procedures for Installation of Suction Caissons in Clay and Other Materials." *Proceedings, Institution of Civil Engineers: Geotechnical Engineering*, **158**(2), 75-82.

Jeanjean, P., Znidarcic, D., Phillips, R., Ko, H.Y., Pfister, S., Cinicioglu, O., Schroeder, K. (2006). "Centrifuge Testing on Suction Anchors: Double-Wall, Over-Consolidated Clay, and Layered Soil Profile." *Proceeding, Annual Offshore Technology Conference*, Paper OTC 18007.

Kulasingam, R. (2003). *"Effects of Void Redistribution on Liquefaction-Induced Deformations."* Ph.D. Thesis, University of California, Davis.

Lacour, M. (2015). "*Learning about Subsea*." <http://milenalacour.com/learn-about-subsea/> (Jul. 13, 2015).

"Photo Gallery." (2009). <http://fishsafe.eu/en/offshore-structures/photo-gallery.aspx.> (Jul. 13, 2015).

Stringer, M.E., Kutter, B.L., Wilson, D.W., Zhou, Y.G., Zheng, B.L. (2012). "*Steel Pile Jacket Seismic Soil Structure Interaction Study: Phase 2 Data Report*." *Technical Report*, Ver. 1.1, University of California, Davis.

Zheng, B.L., Hirt, G.S., Kutter, B.L., Wilson, D.W., Zhou, Y.G. (2014). "*Soil Structure Interaction of Caisson-Supported Subsea Manifold and Wellhead on Soft Clay: Centrifuge Data Report for BLZ02 / PHASE 3-#2*." *Technical Report*, 1.02, University of California, Davis.